Supporting Information

Phosphonium Ylide/Organoaluminum-Based Lewis Pairs for the Highly Efficient Living/controlled Polymerization of Alkyl (Meth)acrylates

Zhikang Chen,[‡a] *Wuchao Zhao,*[‡b] *Conglei Liu,*[a] *Liuying Jiang,*[*a] *Gang Fu,*[a] *Yuetao Zhang,*[*b] *and Hongping Zhu*[*a]

[a] *State Key Laboratory of Physical Chemistry of Solid Surfaces, College of Chemistry and Chemical Engineering, Xiamen University, Xiamen, Fujian, 361005, China*
[b] *State Key Laboratory of Supramolecular Structure and Materials, College of Chemistry, Jilin University, Changchun, Jilin, 130012, China*

Content:

I. X-ray crystallographic analysis

Crystallographic data of compounds LP-**1**, 2 LP-**2** · 2 C_7H_8, LP-**3** · C_7H_8, LPM-**3** · C_6H_6, and LPM-**5** · 0.5 C_7H_8 were all collected on XtaLAB Synergy, Dualflex, HyPix diffractometer (Cu-Kα radiation, λ = 1.54184 Å). Absorption corrections were applied by using the spherical harmonics program (multi-scan type). All structures were solved by direct methods (SHELXS-2015)[1] and refined against F^2 using SHELXL-2017/1.[2] In general, the non-hydrogen atoms were located by difference Fourier synthesis and refined anisotropically, and hydrogen atoms were included using a riding model with U_{iso} tied to the U_{iso} of the parent atoms unless otherwise specified. In 2 LP-**2** · 2 C_7H_8, two independant molecules of LP-**2** were disclosed. One of the two toluene solvent molecules was disordered, which was refined into two parts of C(110)C(111)C(112)C(113)C(114)C(115)C(116) (0.57222) and C(7A)C(1A)C(2A)C(3A)-C(4A)C(5A)C(6A) (0.42778) upon treatment by the PART method. In LP-**3** · C_7H_8, the toluene solvent molecule was disordered, which was refined into two parts of C(53)C(54)C(55)C(56)C(57)C(58)C(59) (0.34621) and C(53A)C(54A)C(55A)C(56A)C(57A)C(58A)C(59A) (0.65379) upon treatment by the PART method. In LPM-**3** · C_6H_6, the ethyl group was disordered that was treated by the PART method and refined into two parts C(5)C(6) and C(5A)C(6A) with the respective occupancies of 0.81371 and 0.18629. The C_6H_6 solvent molecule was seriously disordered and treated by the PART method and refined into three parts C(61)C(62)C(63)C(64)C(65)C(66) (0.25), C(61A)C(62A)C(63A)C(64A)-C(65A)C(66A) (0.50), and C(61B)C(62B)C(63B)C(64B)C(65B)C(66B) (0.25), where C(61B)C(62B)-C(63B)C(64B)C(65B)C(66B) were not able to be performed by the geometric H-atom addition. In LPM-**5** · 0.5 C_7H_8, two independant toluene solvent molecules were disclosed both of 0.25 moiety. A summary of cell parameters, data collection, and structure solution and refinements is given in Table S1.

Table S1. Crystal data and refinements[a]

	LP-**1**	2 LP-**2** · 2 C_7H_8
CCDC number	2232557	2232558
formula	$C_{50}H_{66}AlO_2P$	$C_{116}H_{152}Al_2O_4P_2$
formula weight	756.98	1726.28
crystal system	orthorhombic	triclinic
space group	*Pbca*	*P*–1
a/Å	17.4083(3)	15.9438(4)
b/Å	18.0287(4)	17.9944(3)
c/Å	28.2153(5)	18.5158(4)
α/deg	90	73.892(2)
β/deg	90	88.976(2)
γ/deg	90	88.672(2)
V/Å^3	8855.3(3)	5101.88(19)
Z	8	2
ρ_{calcd}/g·cm^{-3}	1.136	1.124
μ/mm^{-1}	1.016	0.939
F(000)	3280	1872
crystal size/mm^3	0.32x0.28x0.20	0.20x0.20x0.10
θ range/deg	3.13–70.00	2.48–58.78
index ranges	$-21 \le h \le 20$	$-17 \le h \le 17$
	$-21 \le k \le 21$	$-13 \le k \le 19$
	$-34 \le l \le 28$	$-17 \le l \le 20$
collected data	42986	46473
unique data	8359 (R_{int} = 0.0239)	14312 (R_{int} = 0.0197)
completeness to θ	99.5%	98.1%
data/restraints/parameters	8359/0/510	14312/198/1191
GOF on F^2	1.031	1.016
final *R* indices [$I>2\sigma(I)$]	R_1 = 0.0345	R_1 = 0.0378
	wR_2 = 0.0924	wR_2 = 0.0970
R indices (all data)	R_1 = 0.0367	R_1 = 0.0405
	wR_2 = 0.0940	wR_2 = 0.0987
Largest diff peak/hole (e·Å^{-3})	0.350/–0.366	0.520/–0.373

[a]All data were collected at 173(2) K. $R_1 = \sum(||F_o|-|F_c||)/\sum|F_o|$, $wR_2 = \{\sum[w(F_o^2-F_c^2)^2/\sum[w(F_o^2)^2]\}^2\}^{1/2}$, GOF = $\{\sum[w(F_o^2-F_c^2)^2]/(N_o-N_p)\}^{1/2}$.

(continued)

	LP-**3** C_7H_8	LPM-**3** C_6H_6	LPM-**5** 0.5 C_7H_8
CCDC number	2232559	2232560	2232561
formula	$C_{59}H_{78}AlO_2P$	$C_{63}H_{82.5}AlO_4P$	$C_{60.5}H_{82}AlO_4P$
formula weight	877.16	961.74	931.21
crystal system	monoclinic	triclinic	orthorhombic
space group	*P*2(1)/*c*	*P*–1	*Pbca*
a/Å	18.8537(3)	12.6448(2)	12.9446(4)
b/Å	15.5489(2)	15.3492(2)	14.8659(6)
c/Å	18.2578(3)	16.4061(2)	17.9817(7)
α/deg	90	67.9540(10)	109.495(4)
β/deg	103.1110(10)	89.1970(10)	92.100(3)
γ/deg	90	74.8020(10)	107.404(3)
V/Å^3	5212.83(14)	2835.47(7)	3076.5(2)
Z	4	2	2
ρ_{calcd}/g·cm^{-3}	1.118	1.126	1.005
μ/mm^{-1}	0.926	0.919	0.833
F(000)	1904	1041	1010
crystal size/mm^3	0.32x0.26x0.15	0.20x0.20x0.20	0.10x0.10x0.05
θ range/deg	2.41–65.93	2.92–69.98	2.64–58.85
index ranges	$-22 \le h \le 14$	$-15 \le h \le 14$	$-7 \le h \le 14$
	$-18 \le k \le 18$	$-18 \le k \le 18$	$-16 \le k \le 15$
	$-21 \le l \le 21$	$-19 \le l \le 19$	$-19 \le l \le 19$
collected data	60880	66703	25538
unique data	8966 (R_{int} = 0.0236)	10645 (R_{int} = 0.0244)	8588 (R_{int} = 0.0432)
completeness to *θ*	98.9 %	99.1 %	97.3%
data/restraints/parameters	8966/576/624	10645/565/734	8588/576/690
GOF on F^2	1.055	1.023	1.130
final *R* indices [$I > 2\sigma(I)$]	R_1 = 0.0533	R_1 = 0.0343	R_1 = 0.0969
	wR_2 = 0.1449	wR_2 = 0.0907	wR_2 = 0.2643
R indices (all data)	R_1 = 0.0553	R_1 = 0.0351	R_1 = 0.1128
	wR_2 = 0.1466	wR_2 = 0.0913	wR_2 = 0.2786
Largest diff peak/hole (e·Å^{-3})	0.861/–0.687	0.364/–0.296	1.027/–0.397

[a]All data were collected at 173(2) K. $R_1 = \sum(||F_o|-|F_c||)/\sum|F_o|$, $wR_2 = \{\sum[w(F_o^2-F_c^2)^2/\sum[w(F_o^2)^2]\}^{1/2}\}^{1/2}$, GOF = $\{\sum[w(F_o^2-F_c^2)^2]/(N_o-N_p)\}^{1/2}$.

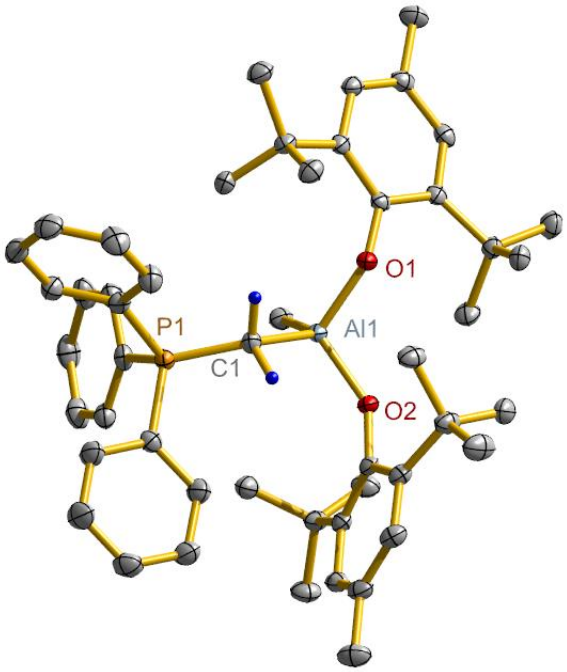

Fig. S1 X-ray crystal structure of LP-**1** with thermal ellipsoids at 50% probability level. The hydrogen atoms except for the CH_2 are omitted for clarity. Selected bond lengths (Å) and angles (°): P1–C1 1.7767(12), C1–Al1 2.0781(13), Al1–O1 1.7682(8), Al1–O2 1.7756(8); P1–C1–Al1 130.96(7), O1–Al1–O2 108.32(4).

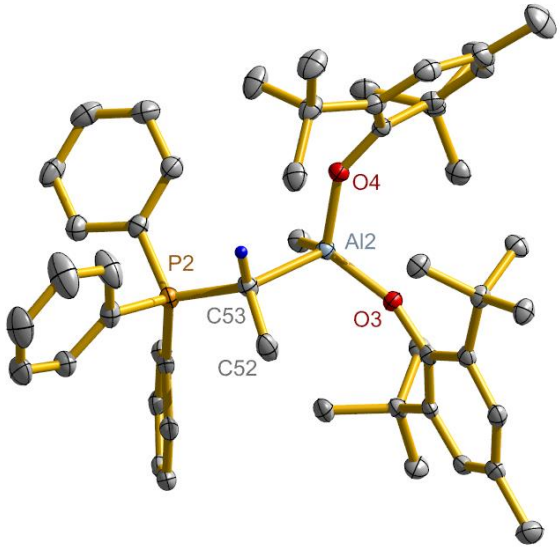

Fig. S2 X-ray crystal structure of another independant molecule of LP-**2** with thermal ellipsoids at 50% probability level. The hydrogen atoms except for the CH are omitted for clarity. Selected bond lengths (Å) and angles (°): P2–C53 1.7805(17), C53–Al2 2.0949(18), Al2–O3 1.7811(12), Al2–O4 1.7569(12); P2–C53–Al2 122.14(9), O3–Al2–O4 112.24(6).

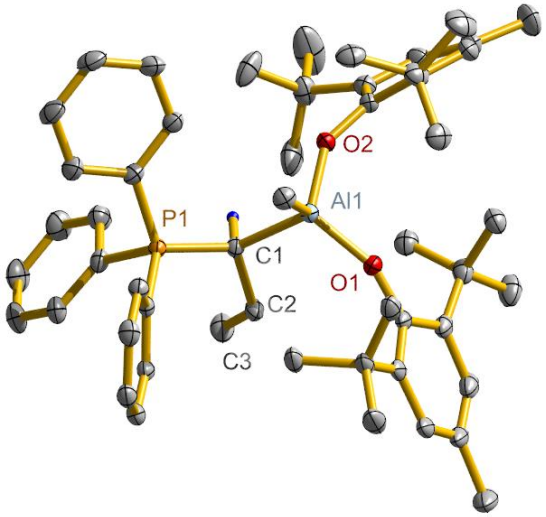

Fig. S3 X-ray crystal structure of LP-**3** with thermal ellipsoids at 50% probability level. The hydrogen atoms except for the CH are omitted for clarity. Selected bond lengths (Å) and angles (°): P1–C1 1.7835(19), C1–Al1 2.1011(19), Al1–O1 1.7601(14), Al1–O2 1.7765(14); P1–C1–Al1 120.86(10), O1–Al1–O2 110.50(7).

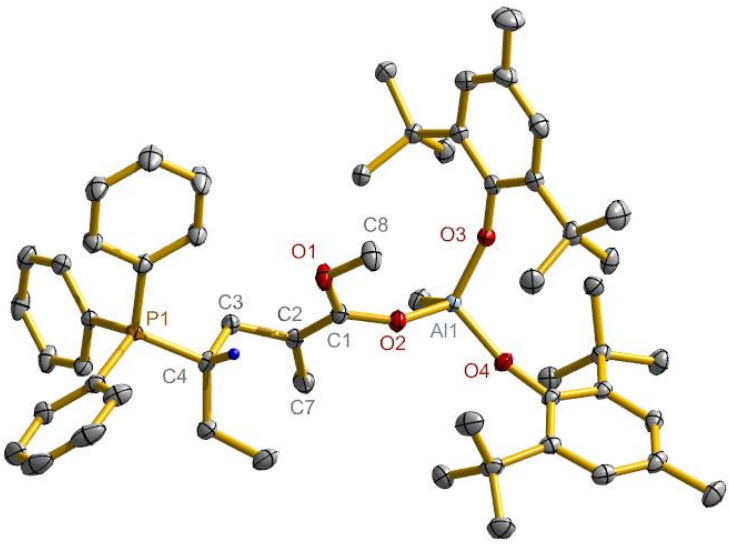

Fig. S4 X-ray crystal structure of LPM-**3** with thermal ellipsoids at 50% probability level. The hydrogen atoms are omitted for clarity. Selected bond lengths (Å) and angles (°): P1–C4 1.8305(11), C4–C3 1.5561(16), C3–C2 1.5108(15), C2–C7 1.5017(17), C2–C1 1.3389(17), C1–O1 1.3880(14), C1–O2 1.3186(14), O1–C8 1.4294(15), Al1–O2 1.7777(8), Al1–O3 1.7531(8), Al1–O4 1.7475(8); P1–C4–C3 109.00(7), C3–C2–C7 117.25(10), O1–C1–O2 115.66(10), O3–Al1–O4 110.32(4), O2–Al1–O3 106.27(4), O2–Al1–O4 105.14(4).

Ⅱ. Study on the relative Lewis acidity strength of the organoaluminum compounds

The Gutmann−Beckett method

The method uses comparison of the ^{31}P NMR resonances of the Et_3PO standard *versus* Et_3PO·LA to determine the Lewis acidity strength of the Al-based LAs, where Et_3PO·$Al(C_6F_5)_3$ was settled as a comparator (100%) instead of Et_3PO·$B(C_6F_5)_3$.[3,4] The same concentration solutions of Et_3PO and Et_3PO·LA each by 0.025 mmol in C_6D_6 (0.5 mL) in a 2-mL NMR tube were employed for the ^{31}P NMR measurement, where Et_3PO·LA was obtained by *in-situ* mixing Et_3PO and equivalent LA. The solution obtained was kept after 30 min at room temperature (298 K) prior to test.

Table S2. The relative Lewis acidity data obtained through the Gutmann−Beckett method

compound	$^{31}P\{^1H\}$ (δ/ppm)	$\Delta\delta$ values relative to that of free Et_3PO (δ/ppm)	relative Lewis acidity (%)
Et_3PO	46.0	0	–
Et_3PO·$Al(C_6F_5)_3$	75.3	29.3	100%
Et_3PO·$AlMe(BHT)_2$	69.5	23.5	80%
Et_3PO·$AlEt(BHT)_2$	69.3	23.3	79%
Et_3PO·$Ali\text{Bu}(BHT)_2$	69.3	23.3	79%
Et_3PO·$Ali\text{Bu}_2(BHT)$	66.2	20.2	69%

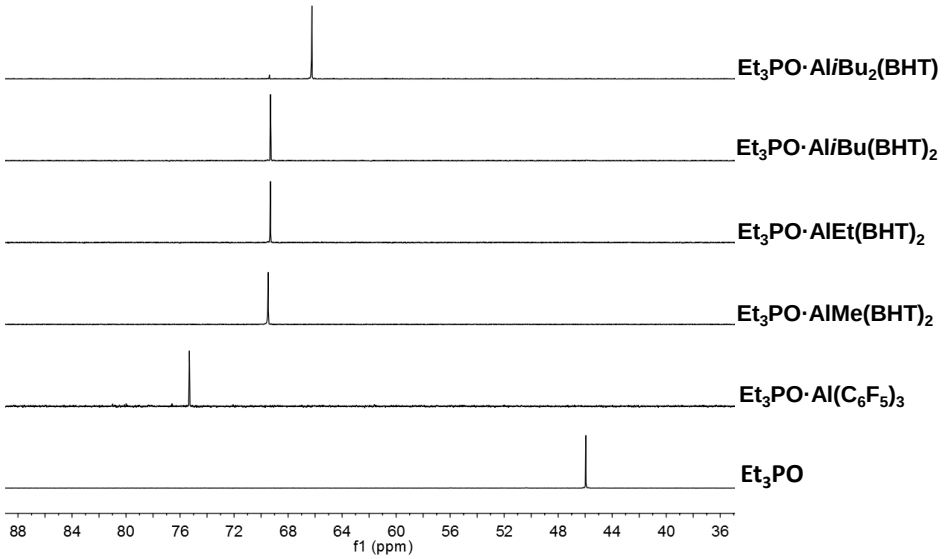

Fig. S5 The ^{31}P NMR spectra profile for Et_3PO and Et_3PO·LAs measured in C_6D_6 at 298 K.

Ⅲ. Study on the relative Lewis basicity strength of the P-ylide compounds

1. NBO analysis and computational details

Density functional theory calculations were performed using M06-2X[5] with the 6-311+G(3d,2p) basis sets to all atoms of the P-ylide molecules.[6,7] Geometries were fully optimized, and vibrational frequencies were calculated to ensure no other imaginary frequency at a native minimum of the molecules studied. The charge analyses were performed with the natural bond orbital (NBO) scheme.[8–13]

All calculations were carried out using the Gaussian 09 package.[14]

The charge distributions at the atoms for the P=C bond of the P-ylides were calculated (Table S3), which indicate that the P-atom holds the positive charge by 1.593, 1.613, 1.619, 1.635, and 1.631 whereas the C-atom the negative charge by –1.219, –0.984, –0.980, –0.922, and –0.785 corresponding from P-ylide-**1** to P-ylide-**5**, respectively. This implies that the nucleophilic reactivity is settled at the C-atom, with strength in better sequence decreasing from P-ylide-**1** to P-ylide-**5**.

Table S3. The charge distributions calculated at the atoms for the P=C bond of the P-ylides

$Ph_3P{=}CR_2$

compound	R_2	P	C
P-ylide-**1**	H,H	1.593	–1.219
P-ylide-**2**	H,Me	1.613	–0.984
P-ylide-**3**	H,Et	1.619	–0.980
P-ylide-**4**	H,Ph	1.635	–0.922
P-ylide-**5**	Me,Me	1.631	–0.785

2. ^{31}P NMR spectral analysis of P-ylide-1–P-ylide-5

The ^{31}P NMR spectra analysis show resonances at δ 21.20, 14.57, 12.31, 7.79, and 9.86 corresponding from P-ylide-**1** to P-ylide-**5**, respectively. These data indicate variation of the phosphorus resonances of the five P-ylides due to change of the substituents at P=C carbon atom, as appears little influence direct to the nucleophilic reactivity strength at the C-atom.

Table S4. The ^{31}P NMR data measured for P-ylides

compound	$^{31}P\{^{1}H\}$ NMR (δ/ppm)
P-ylide-**1**	21.20
P-ylide-**2**	14.57
P-ylide-**3**	12.31
P-ylide-**4**	7.79
P-ylide-**5**	9.86

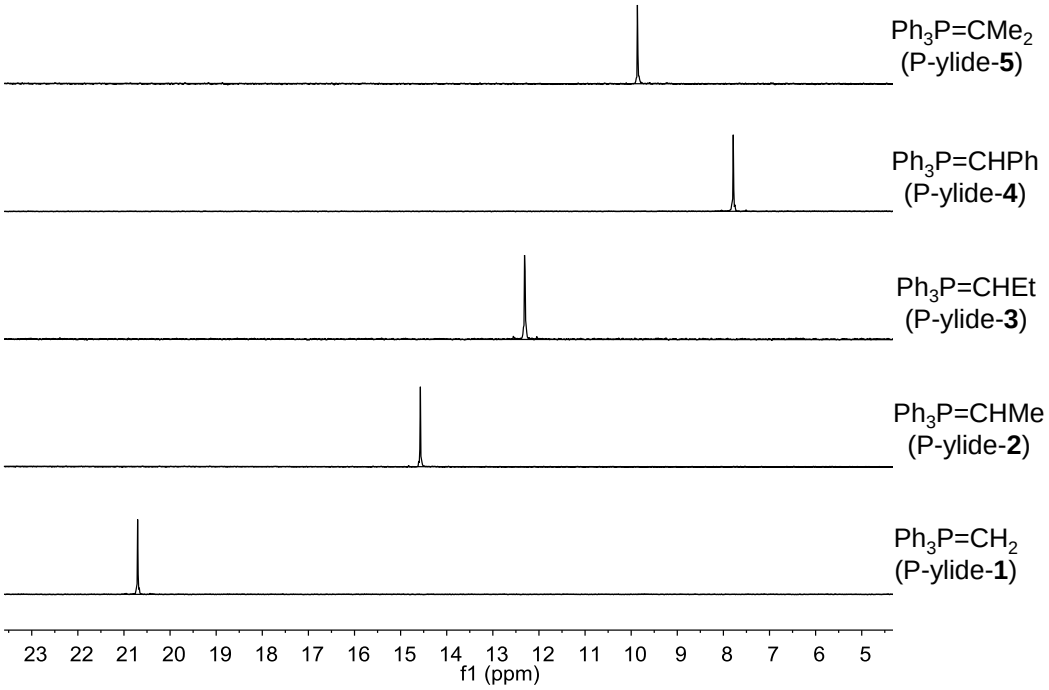

Fig. S6 The ^{31}P NMR spectra profile for P-ylide-**1**–P-ylide-**5** measured in C_6D_6 at 298 K.

3. ^{31}P NMR spectral analysis on reactions of P-ylide-1–P-ylide-5 each with AlMe(BHT)$_2$

As seen from Fig. S7, reactions of P-ylide-**1**–P-ylide-**3** each with AlMe(BHT)$_2$ resulted in formation of LP-**1**–LP-**3**. No reaction happened between P-ylide-**4** and AlMe(BHT)$_2$ whereas complex reaction occurred for P-ylide-**5** and AlMe(BHT)$_2$. The LP-**1**–LP-**3** are of the classical Lewis pair (CLP) character whereas P-ylide-**4** and AlMe(BHT)$_2$ form a frustrated Lewis pair (FLP). These results detect varied interactions between the P-ylides and AlMe(BHT)$_2$.

Table S5. The ^{31}P NMR data measured for reactions of P-ylide-**1**–P-ylide-**5** with AlMe(BHT)$_2$

reaction	^{31}P{^{1}H} NMR (δ/ppm)
P-ylide-**1** + AlMe(BHT)$_2$	32.00 (LP-**1**)
P-ylide-**2** + AlMe(BHT)$_2$	37.01 (LP-**2**)
P-ylide-**3** + AlMe(BHT)$_2$	35.11 (LP-**3**)
P-ylide-**4** + AlMe(BHT)$_2$	7.79 (P-ylide-**4**)
P-ylide-**5** + AlMe(BHT)$_2$	41.75 (27%, LP-**5**), 40.67 (2%, unknown), 39.32 (2%, unknown), 32.35 (15%, unknown), 30.87 (3%, unknown), 9.92 (10%, P-ylide-**5**), –5.36 (41%, unknown)

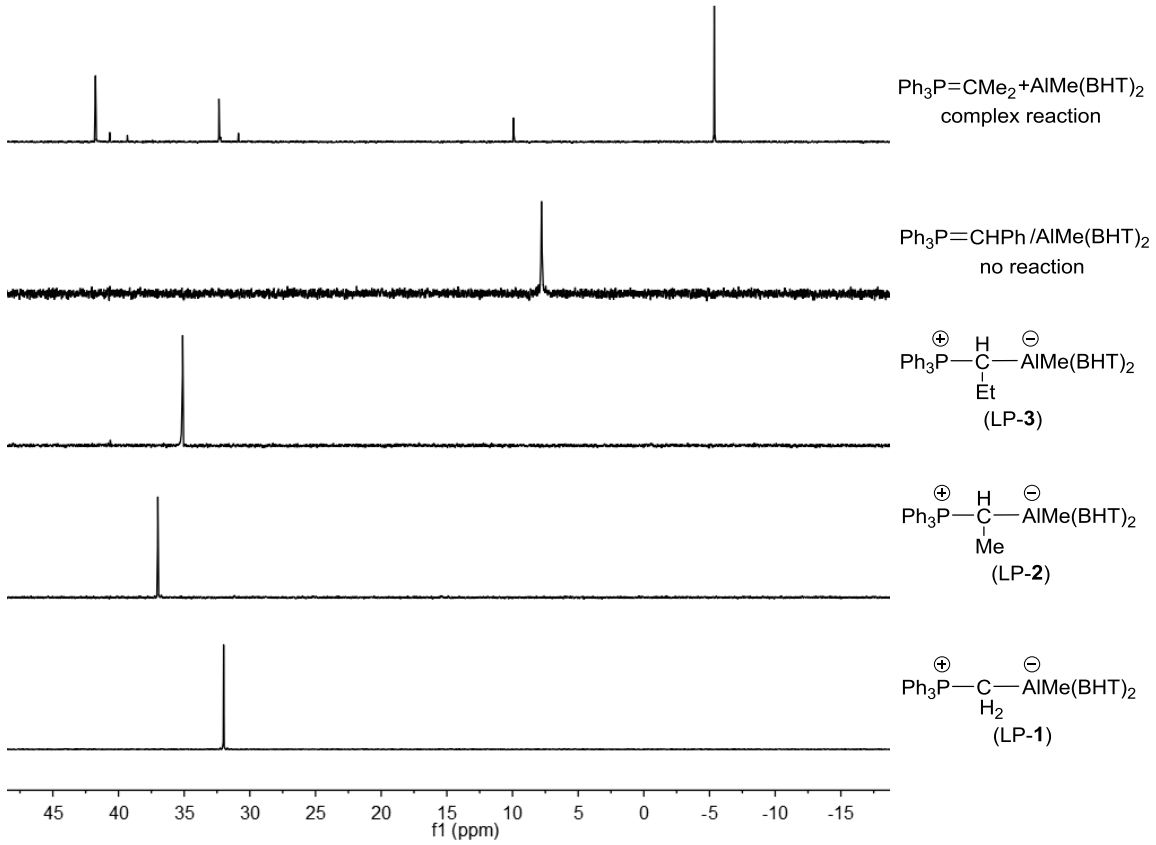

Fig. S7 The ^{31}P NMR spectra profile for reactions of P-ylide-**1**–P-ylide-**5** with AlMe(BHT)$_2$ measured in C_6D_6 at 298 K.

4. ^{31}P NMR spectral analysis on reactions of P-ylide-1–P-ylide-5 each with MMA ·AlMe(BHT)$_2$

As seen from Fig. S8 and Table S6, reaction of P-ylide-**1** with MMA ·AlMe(BHT)$_2$ produced LPM-**1** as minor part while LP-**1** as the major one. Reactions of either P-ylide-**2** or P-ylide-**3** with AlMe(BHT)$_2$ gave completely LPM-**2** or LPM-**3**. And reactions of P-ylide-**4** and P-ylide-**5** each with AlMe(BHT)$_2$ generated besides LPM-**4** and LPM-**5** the unknown species. These results detect influence due to change of the P-ylides.

Table S6. The ^{31}P NMR data measured for reactions of P-ylide-**1**–P-ylide-**5** each with MMA ·$AlMe(BHT)_2$

reaction	$^{31}P\{^1H\}$ NMR (δ/ppm)
P-ylide-**1** + MMA ·$AlMe(BHT)_2$	31.95 (80%, LP-**1**), 25.18 (4%, *cis*-LPM-**1**), 24.65 (16%, *trans*-LPM-**1**)
P-ylide-**2** + MMA ·$AlMe(BHT)_2$	27.56 (*trans*-LPM-**2**)
P-ylide-**3** + MMA ·$AlMe(BHT)_2$	29.42 (18%, *cis*-LPM-**3**), 28.77 (82%, *trans*-LPM-**3**)
P-ylide-**4** + MMA ·$AlMe(BHT)_2$	24.01 (12%, *cis*-LPM-**4**), 20.90 (69%, *trans*-LPM-**4**), –5.49 (19%, unknown)
P-ylide-**5** + MMA ·$AlMe(BHT)_2$	35.66 (95%, *trans*-LPM-**5**), –5.34 (5%, unknown)

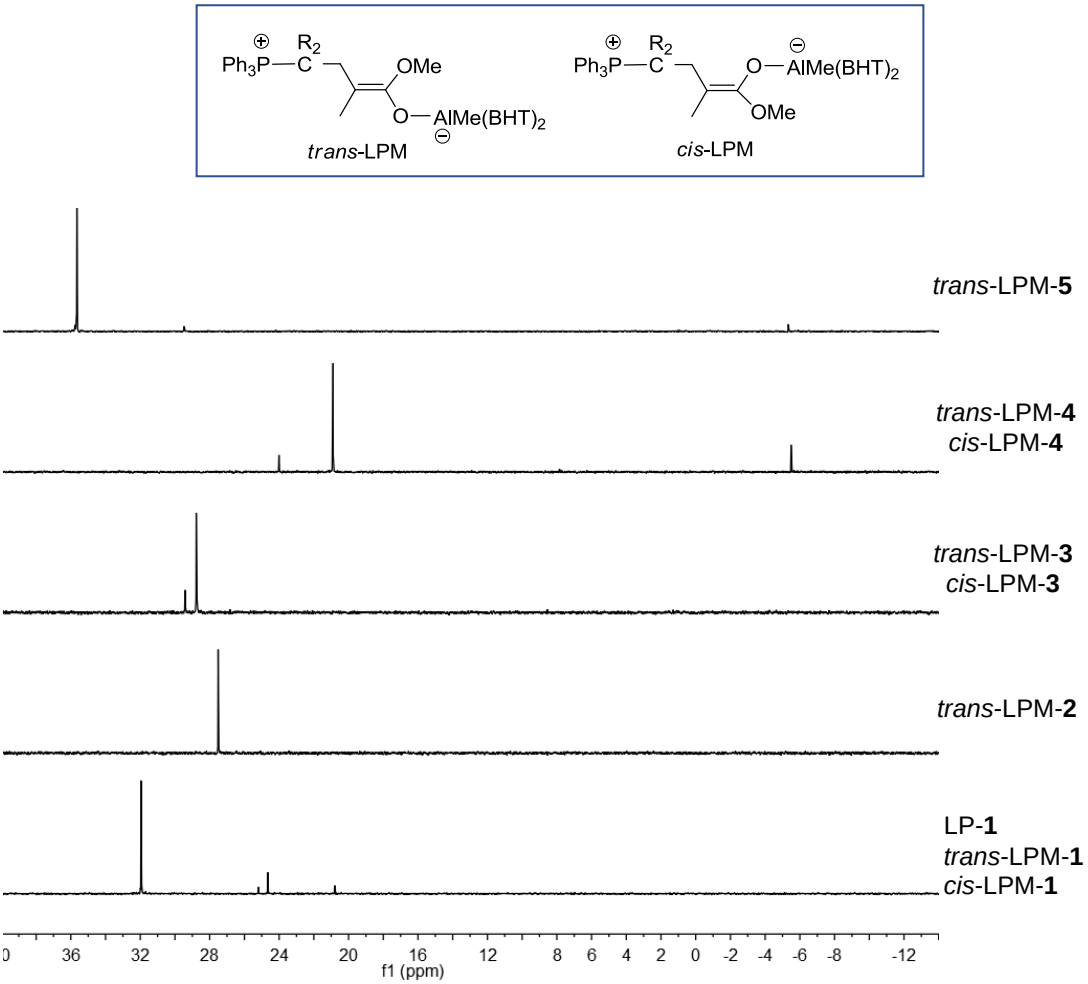

Fig. S8 The ^{31}P NMR spectra profile for reactions of P-ylide-**1**–P-ylide-**5** each with MMA ·$AlMe(BHT)_2$ measured in C_6D_6 at 298 K (Note: detailed assignemnts are seen in Fig.s S25, S27, S29, S31, and S33 in VI).

Ⅳ. Some other polymerization results

Table S7. The MMA polymerization results by using only the P-ylide initiators[a]

Run	LB	[MMA]:[LB]	*t* (h)	Conv.[b] (%)
1	P-ylide-**1**	200:1	24	2.0
2	P-ylide-**2**	200:1	24	4.7
3	P-ylide-**3**	200:1	24	3.8
4	P-ylide-**4**	200:1	24	0
5	P-ylide-**5**	200:1	24	9.0

[a]Conditions: MMA 4.6 mmol, toluene 5 mL, at 298 K. [b]Monomer conversion was calculated according to the ^{1}H NMR data measured.

Table S8. The copolymerization results by using the P-ylide-**2**/Al*i*Bu$_2$(BHT) initiator system[a]

run	[P-ylide-**2**]:[Al*i*Bu$_2$(BHT)]:[M]	*t* (min)	Conv.[b] (%)	M_n[c] (kg/mol)	$Đ$[c]
1	1:2:(200 MMA/200 MMA)	5	>99	46.9	1.19
2	1:2:(200 MMA/200 EMA)	5	>99	53.2	1.18
3	1:2:(200 MMA/200 BnMA)	5	>99	83.8	1.05
				30.5	1.02
4	1:2:(200 MMA/200 *n*BuMA)	5	>99	76.6	2.28

[a]Conditions: carried out at 298 K in toluene (10 mL); first monomer (MMA) 4.6 mmol, second monomer 4.6 mmol. [b]Monomer conversions were calculated according to ^{1}H NMR data measured. [c]M_n and $Đ$ determined by GPC relative to PMMA standards in THF.

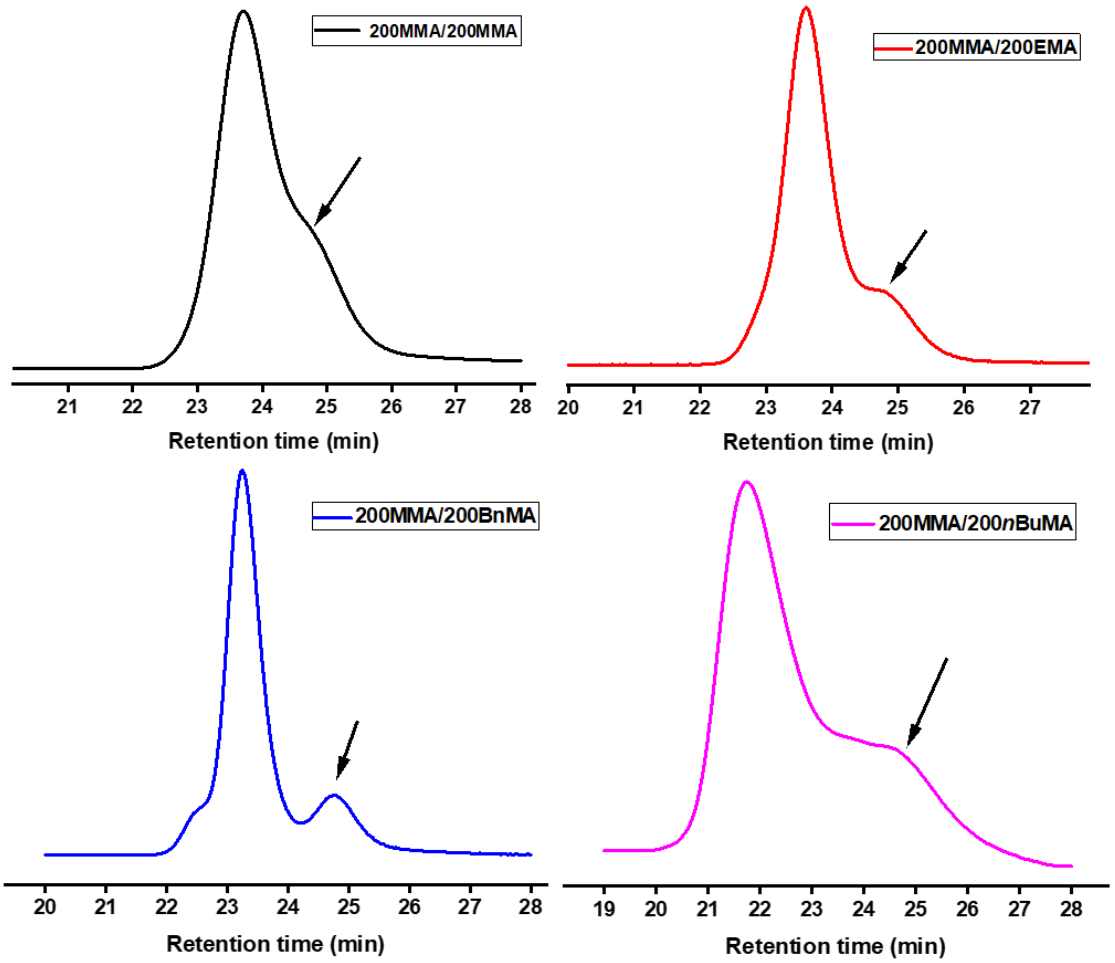

Fig. S9 The GPC traces of PMMA samples obtained from chain-extension and copolymerization experiments by using the P-ylide-**2**/Al*i*Bu$_2$(BHT) initiator system.

Table S9. The chain-extension polymerization results by using the P-ylide-**2**/AlMe(BHT)$_2$ initiator system[a]

run	[P-ylide-**2**]:[AlMe(BHT)$_2$]:[M]	Conv.[b] (%)	M_n[c] (kg/mol)	$Đ$[c]	I*[d] (%)
1	1:2:(200 MMA)	>99	31.7	1.18	64
2	1:2:(200 MMA/200 MMA)	>99	51.4	1.16	78
3	1:2:(200 MMA/200 MMA/200 MMA)	>99	71.1	1.12	85

[a]Condition: carried out at 298 K in toluene; [MMA] = 0.92 M. [b]Monomer conversions were calculated according to ^{1}H NMR data measured. [c]M_n and $Đ$ determined by GPC relative to PMMA standards in THF. [d]Initiator efficiency (I*) = M_n(calcd)/M_n(exptl), where M_n(calcd) = [MW(MMA)]([MMA]$_0$/[I]$_0$) (conversion %) + MW of chain-end groups.

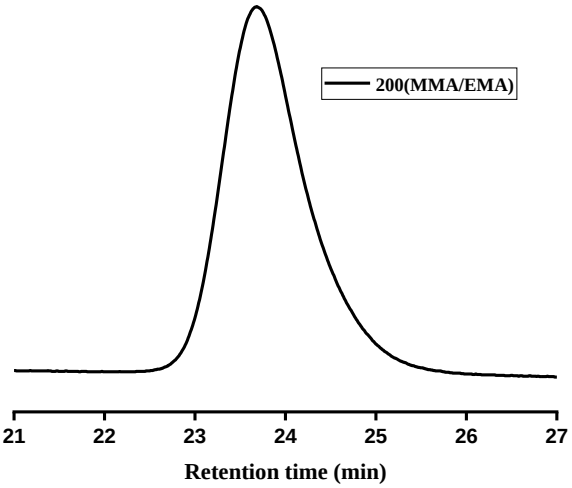

Fig. S10 The GPC trace of the PMMA sample obtained from random copolymerization by using the P-ylide-**2**/AlMe(BHT)$_2$ initiator system (run 10, Table 2).

V. Other collected MALDI-TOF MS spectra

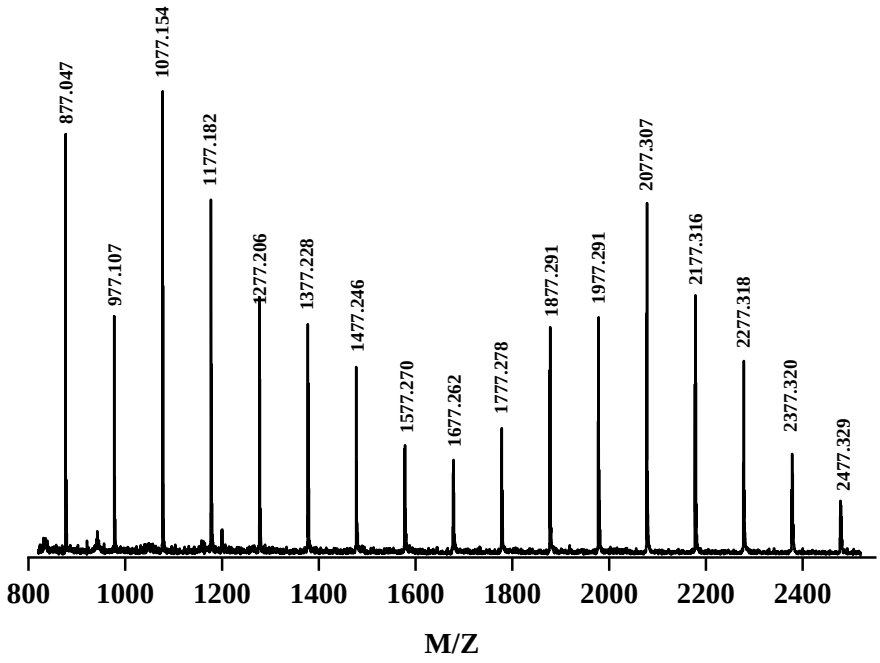

Fig. S11 MALDI-TOF MS spectrum of the low-MW PMMA sample produced by P-ylide-**1**/AlMe(BHT)$_2$ in toluene at 298 K.

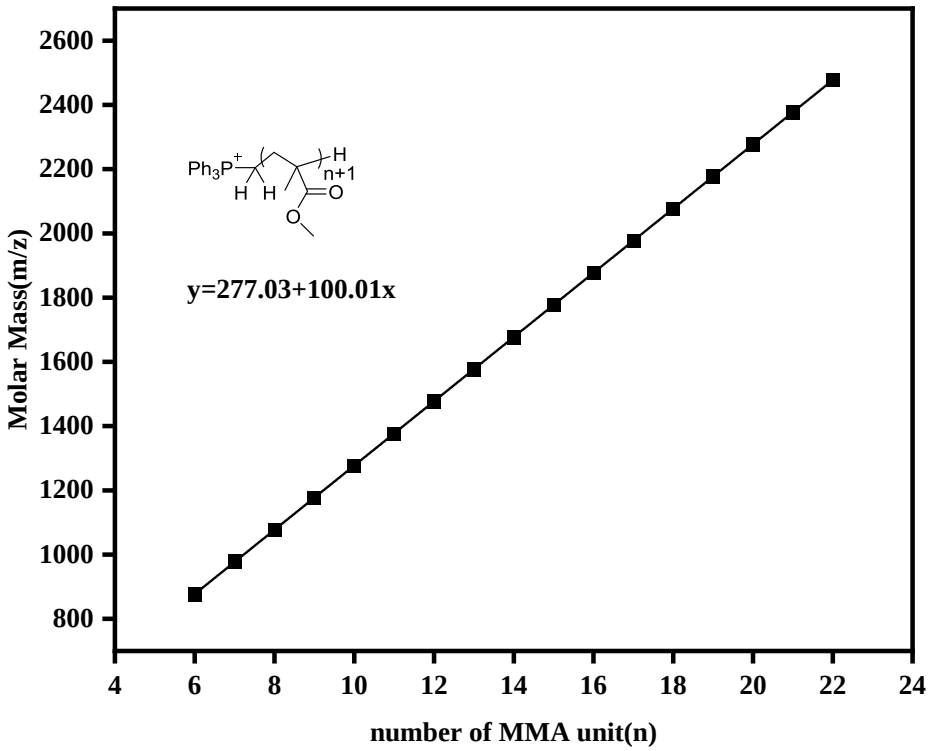

Fig. S12 Plot of *m*/*z* values from Fig. 11 *vs* the number of MMA repeat units (*n*).

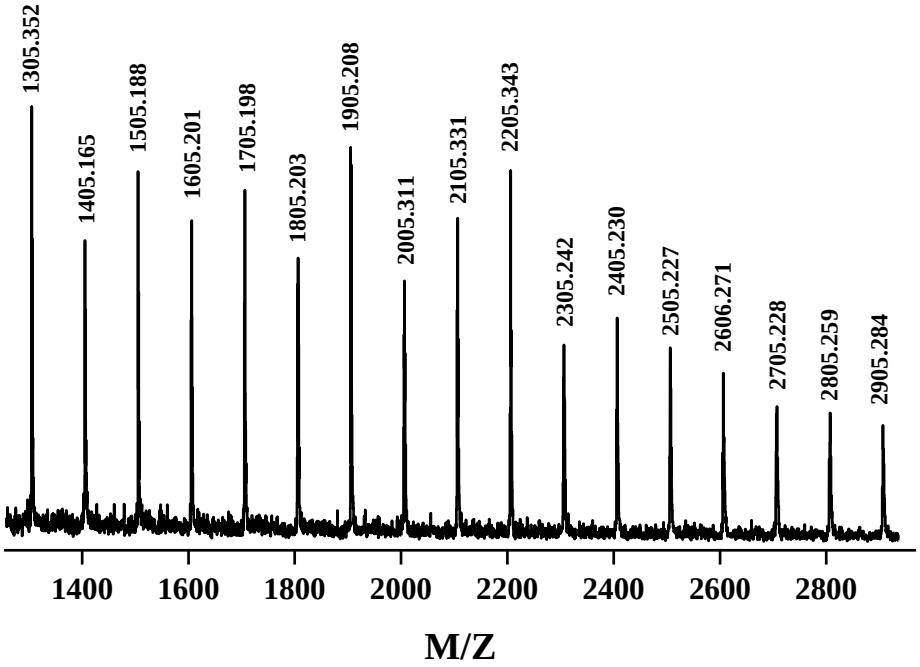

Fig. S13 MALDI-TOF MS spectrum of the low-MW PMMA sample produced by P-ylide-**3**/AlMe(BHT)$_2$ in toluene at 298 K.

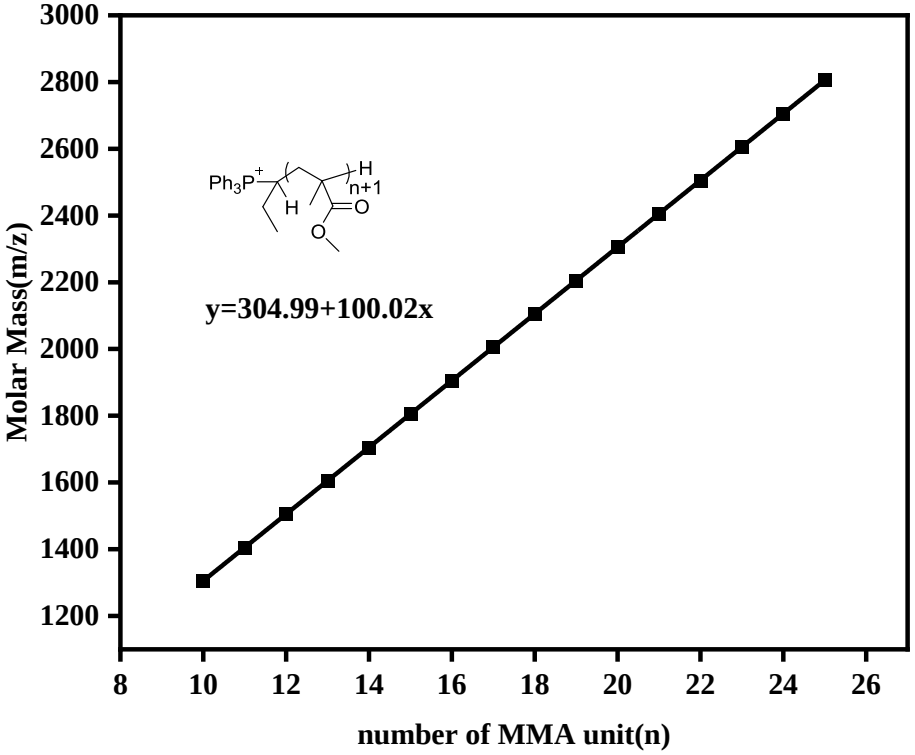

Fig. S14 Plot of *m*/*z* values from Fig. S13 vs the number of MMA repeat units (*n*).

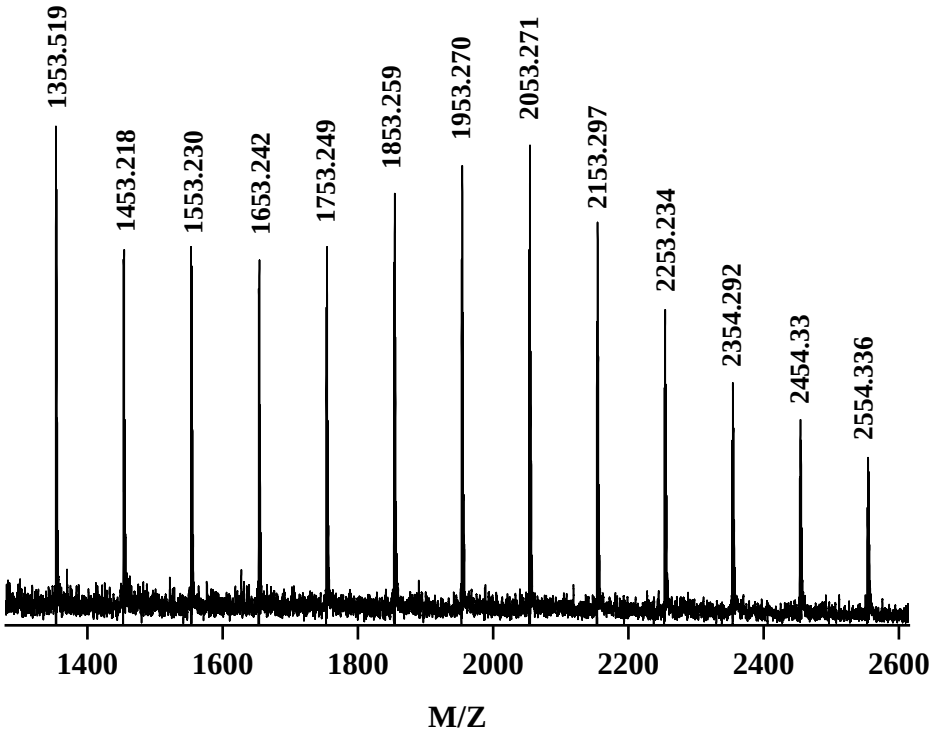

Fig. S15 MALDI-TOF MS spectrum of the low-MW PMMA sample produced by P-ylide-**4**/AlMe(BHT)$_2$ in toluene at 298 K.

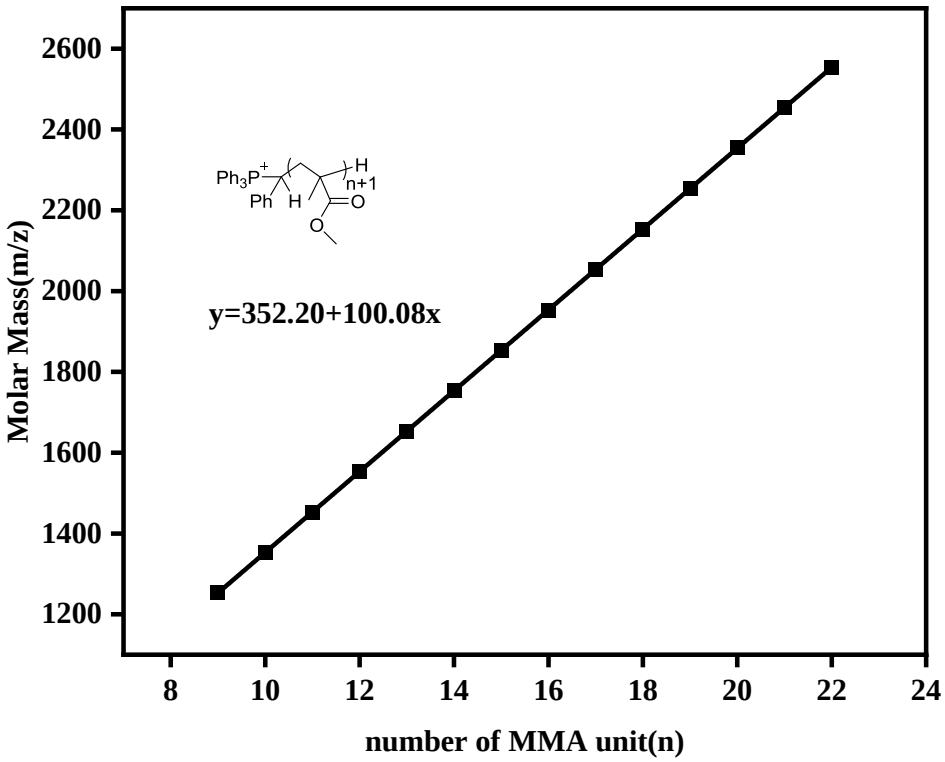

Fig. S16 Plot of *m*/*z* values from Fig. S15 *vs* the number of MMA repeat units (*n*).

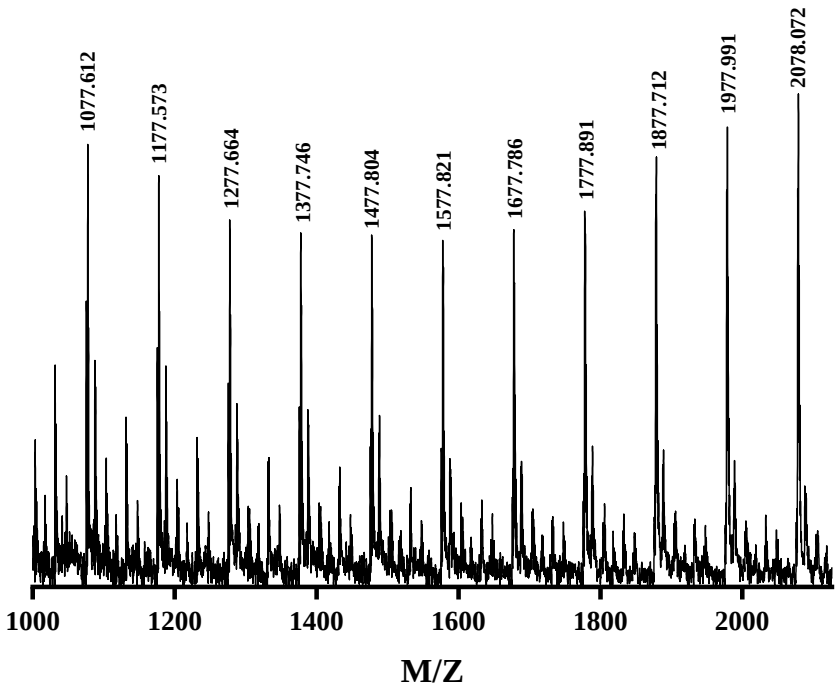

Fig. S17 MALDI-TOF MS spectrum of the low-MW PMMA sample produced by P-ylide-**1**/Al*i*Bu$_2$(BHT) in toluene at 298 K.

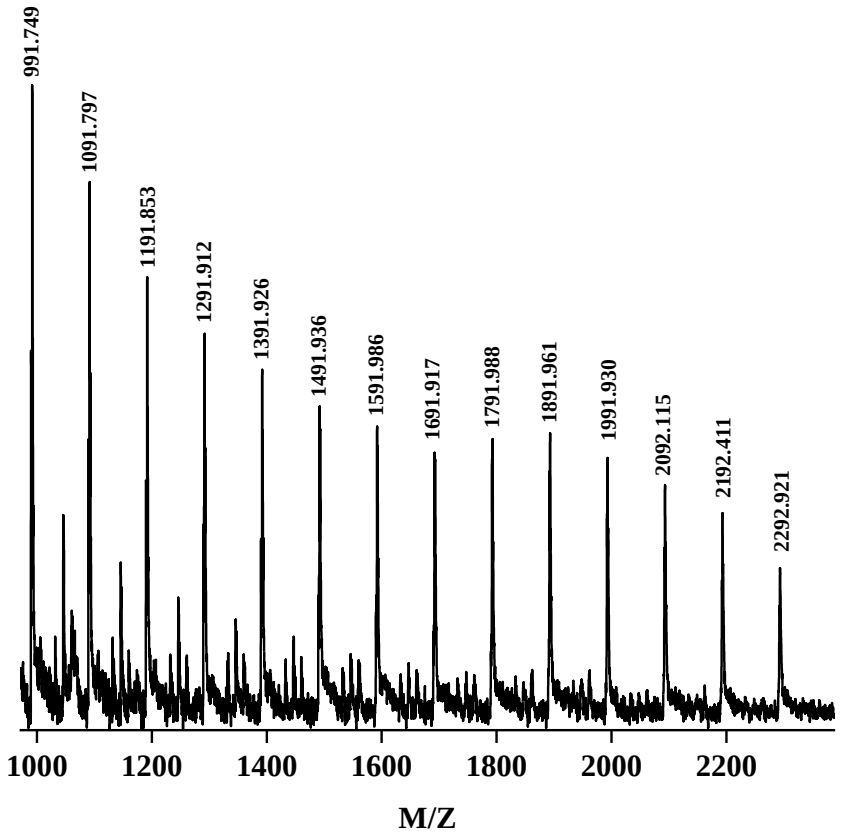

Fig. S18 MALDI-TOF MS spectrum of the low-MW PMMA sample produced by P-ylide-**2**/Al*i*Bu_2(BHT) in toluene at 298 K.

Ⅵ. Collected NMR (^{1}H and ^{31}P) spectra

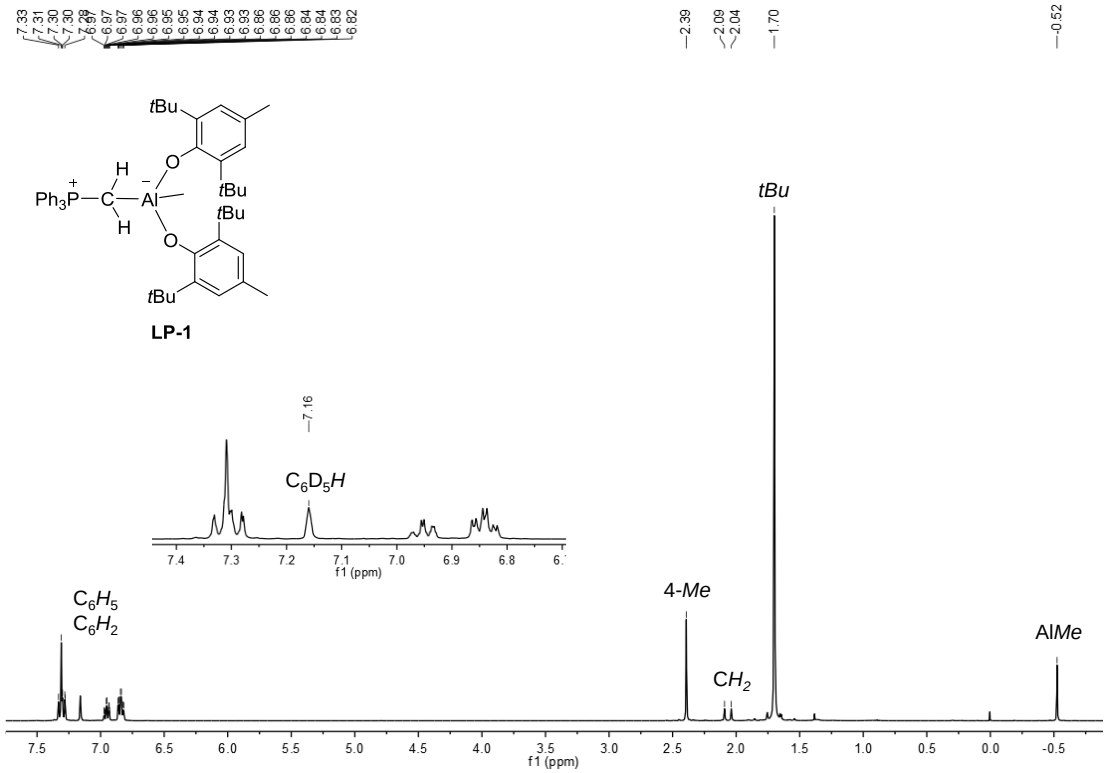

Fig. S19 ^{1}H NMR spectrum of LP-**1** in C_6D_6 at 298 K

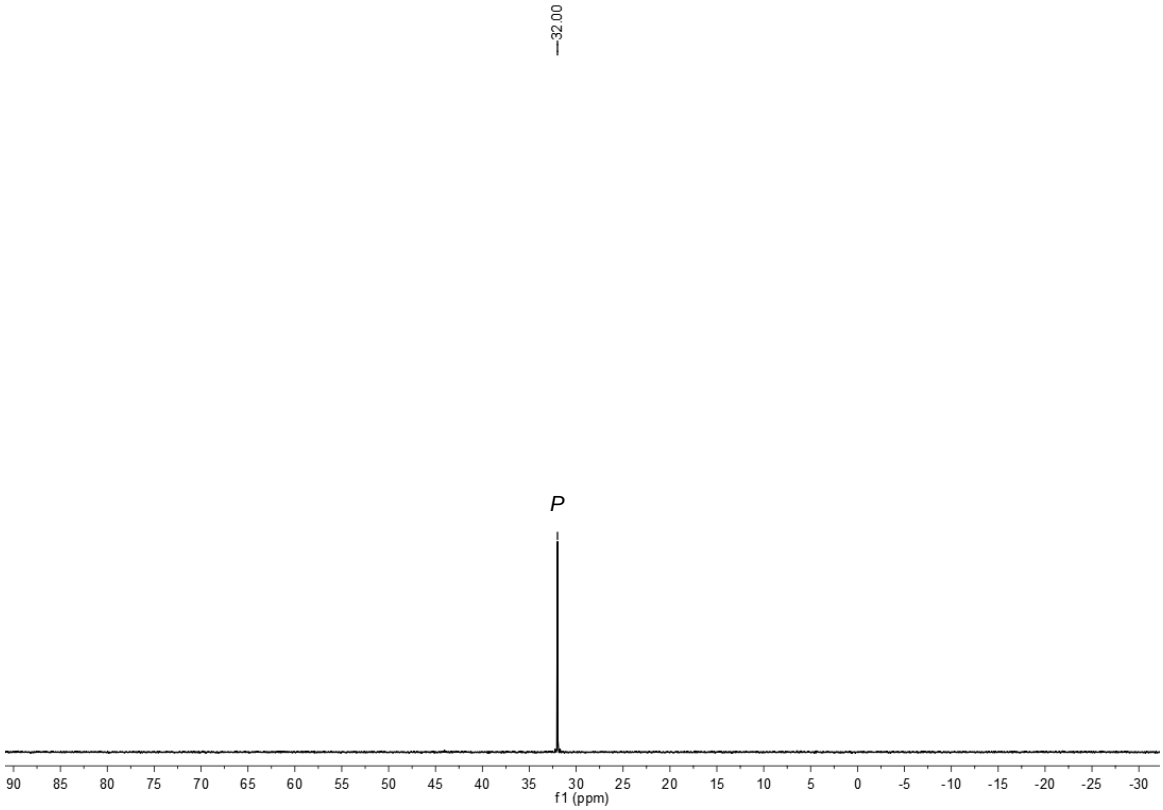

Fig. S20 ^{31}P NMR spectrum of LP-**1** in C_6D_6 at 298 K

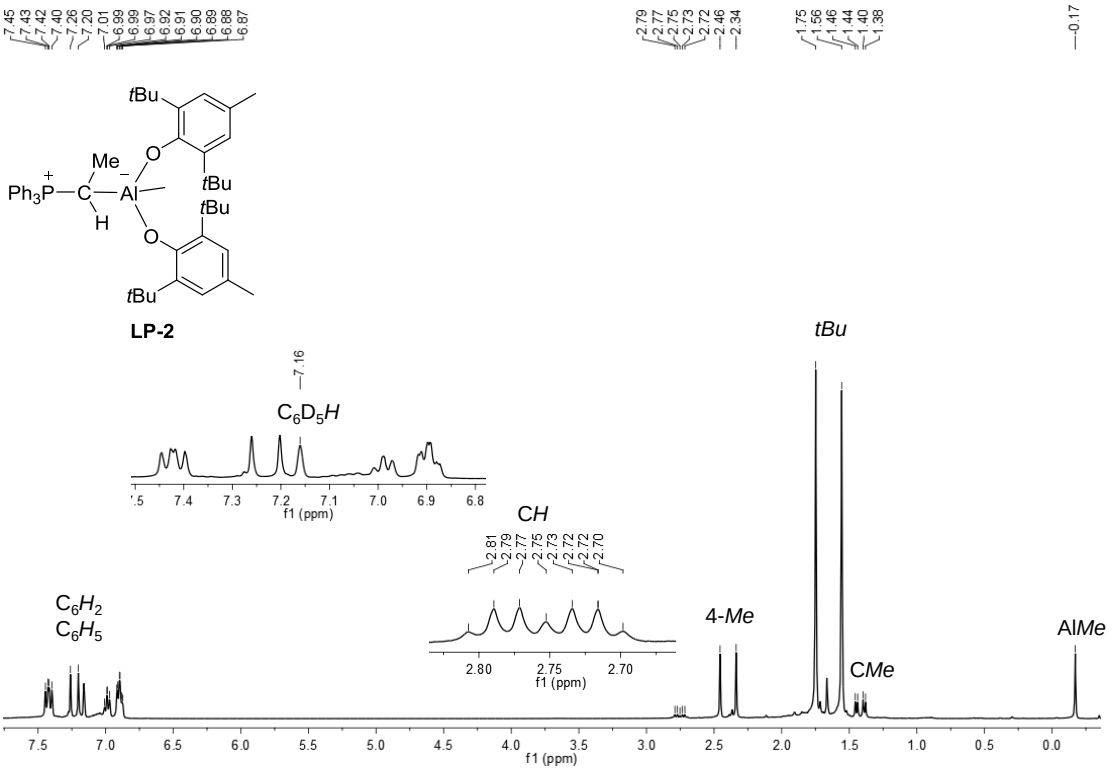

Fig. S21 ^{1}H NMR spectrum of LP-**2** in C_6D_6 at 298 K

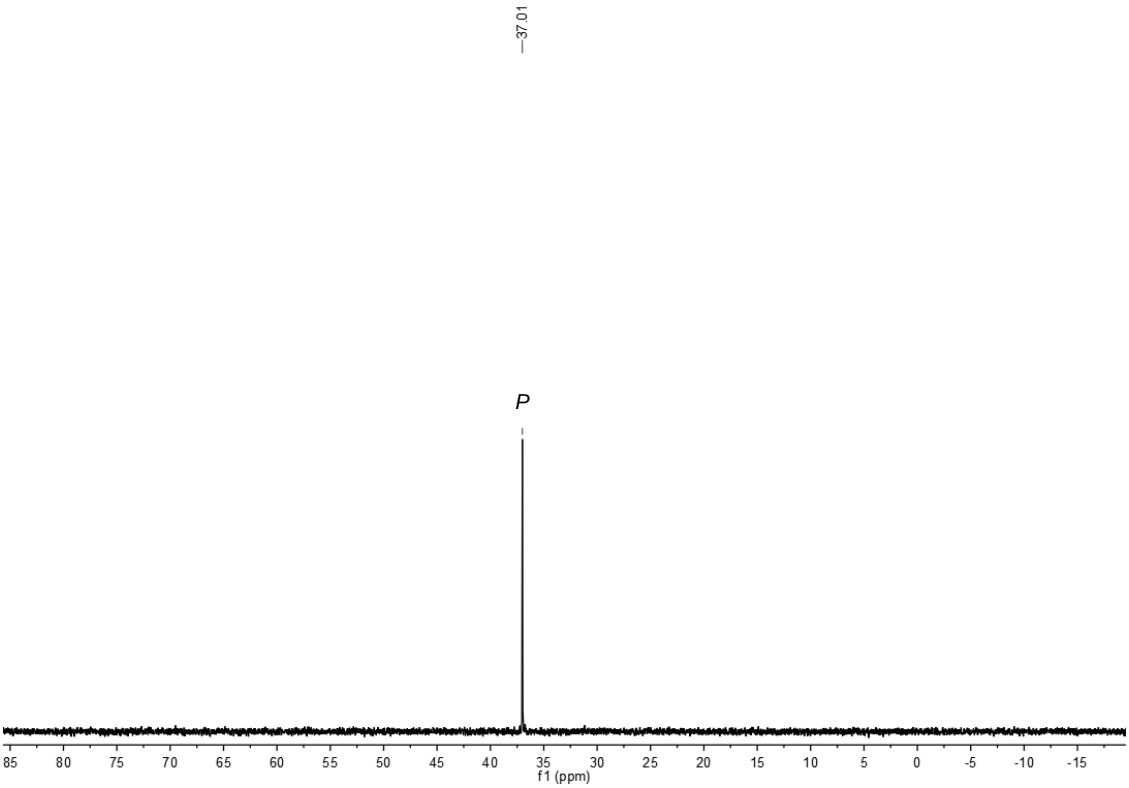

Fig. S22 ^{31}P NMR spectrum of LP-**2** in C_6D_6 at 298 K

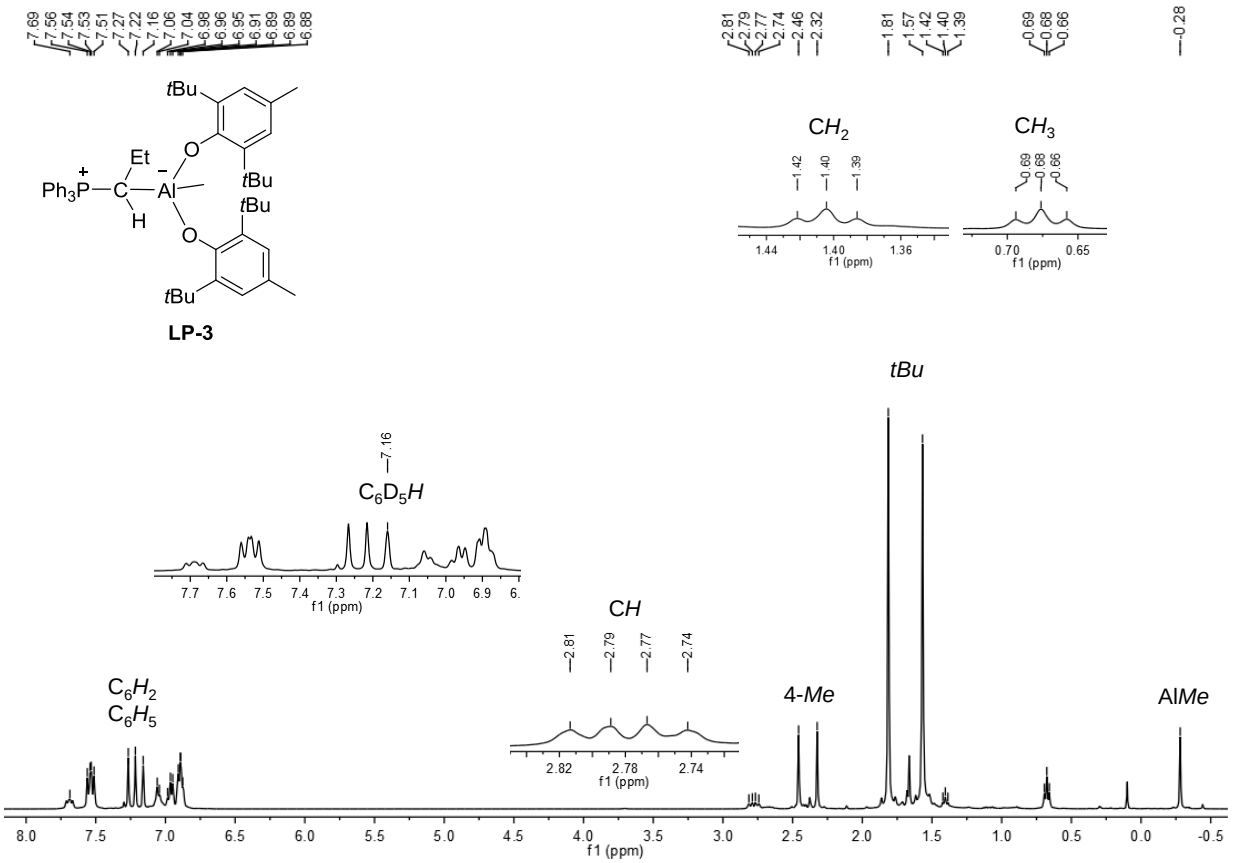

Fig. S23 ^{1}H NMR spectrum of LP-**3** in C_6D_6 at 298 K

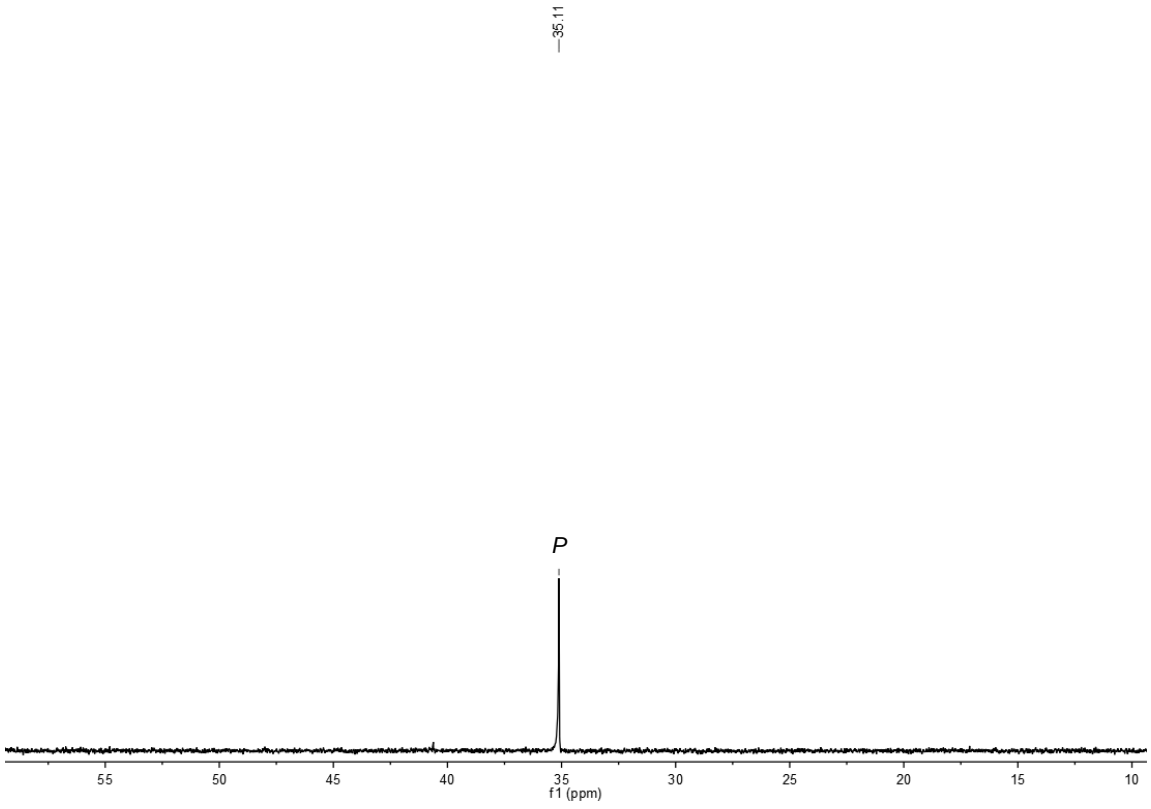

Fig. S24 ^{31}P NMR spectrum of LP-**3** in C_6D_6 at 298 K

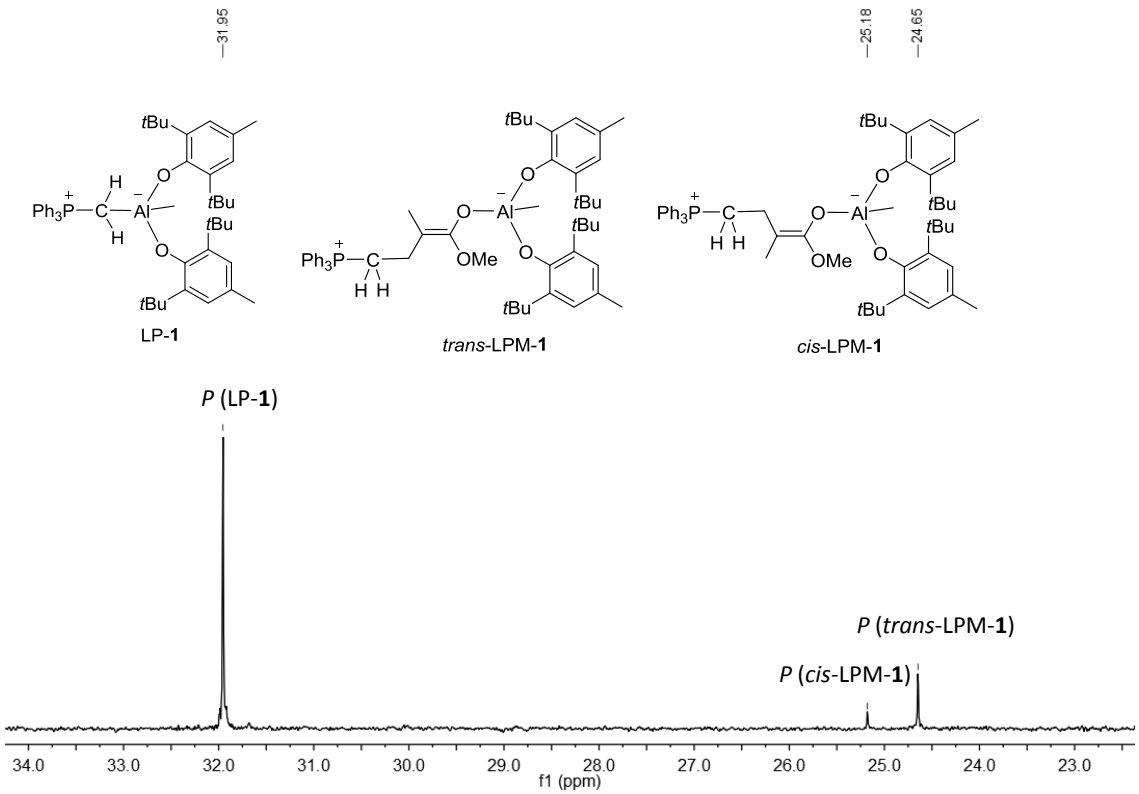

Fig. S25 ^{31}P NMR spectrum of LPM-**1** in C_6D_6 at 298 K

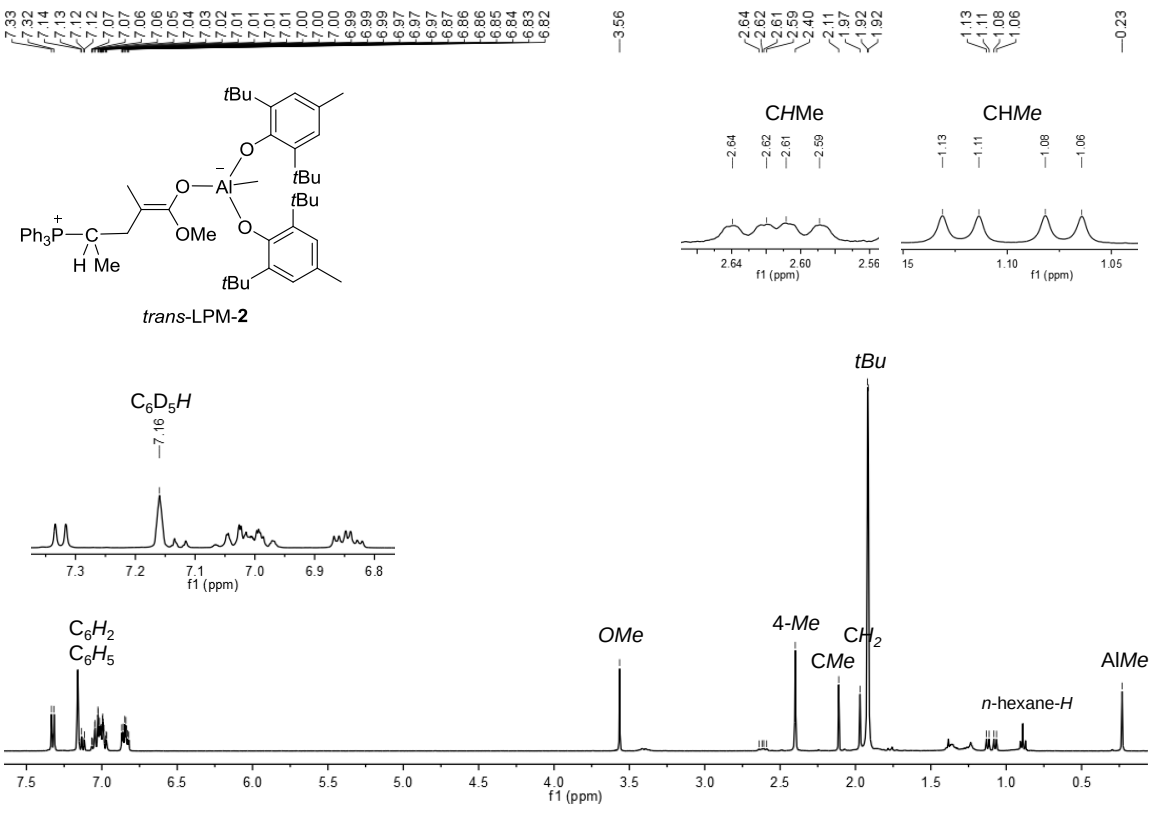

Fig. S26 ^{1}H NMR spectrum of LPM-**2** in C_6D_6 at 298 K

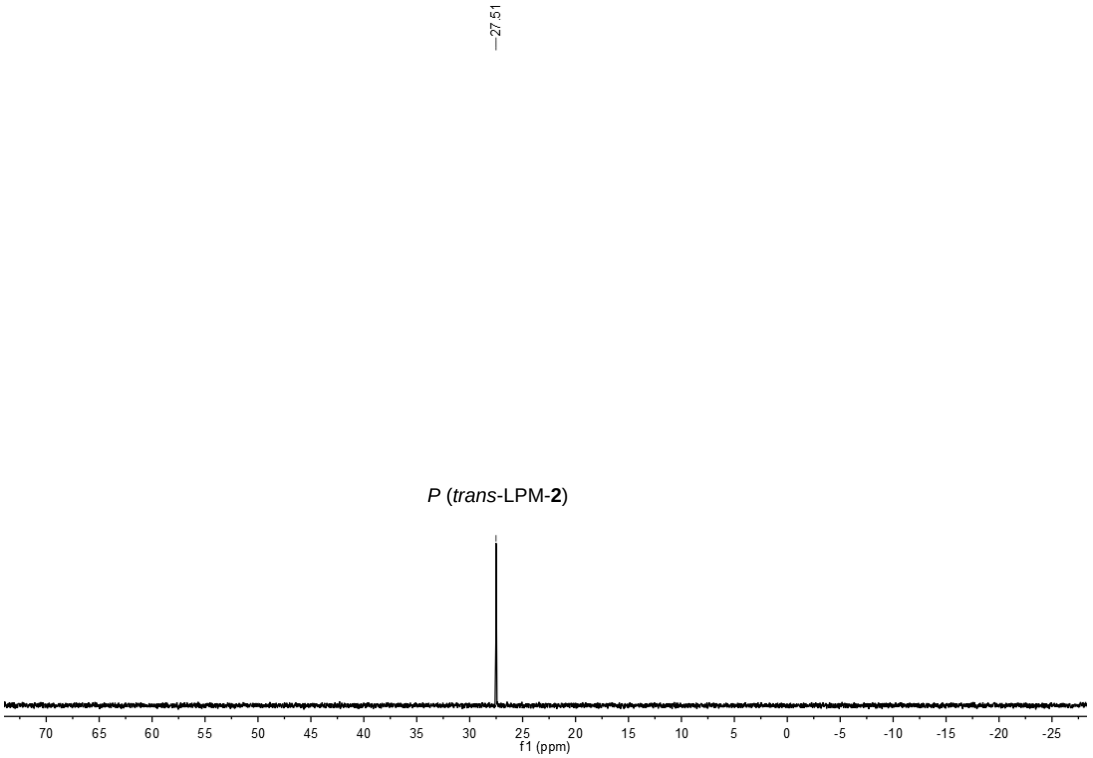

Fig. S27 ^{31}P NMR spectrum of LPM-**2** in C_6D_6 at 298 K

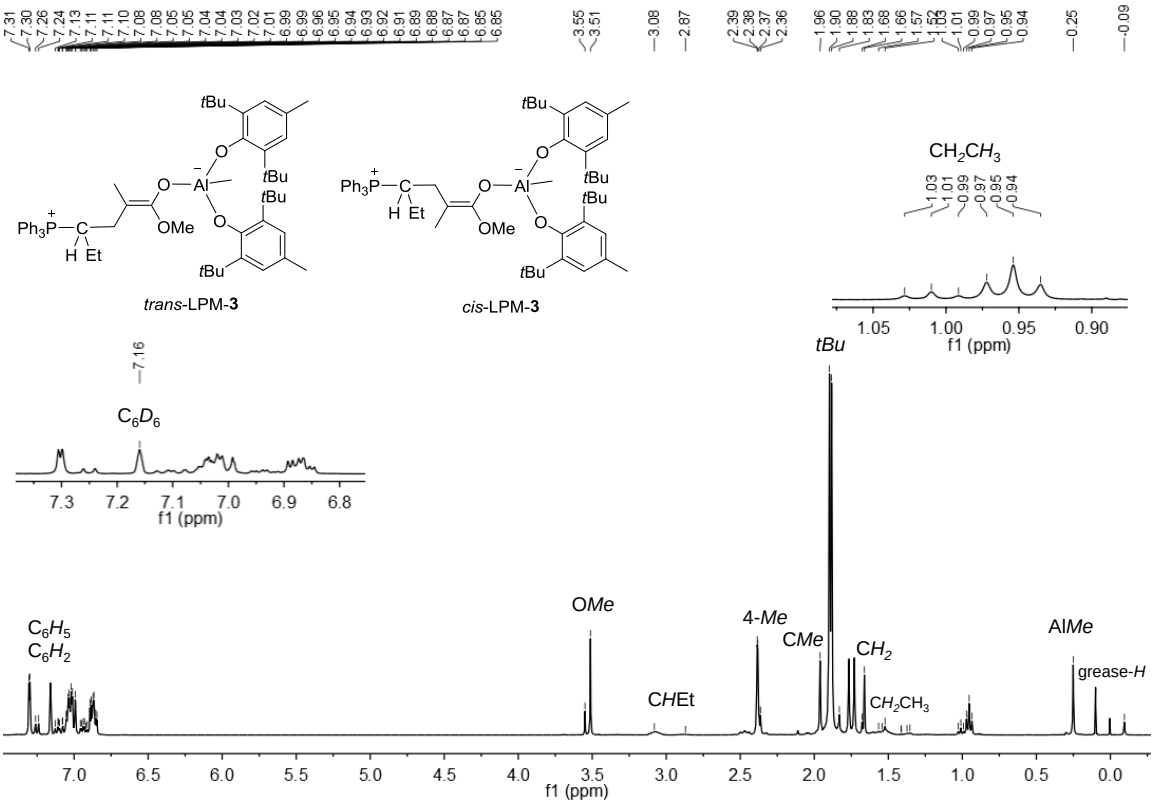

Fig. S28 ^{1}H NMR spectrum of LPM-**3** in C_6D_6 at 298K (Note: the data were labeled for *trans*-LPM-**3**)

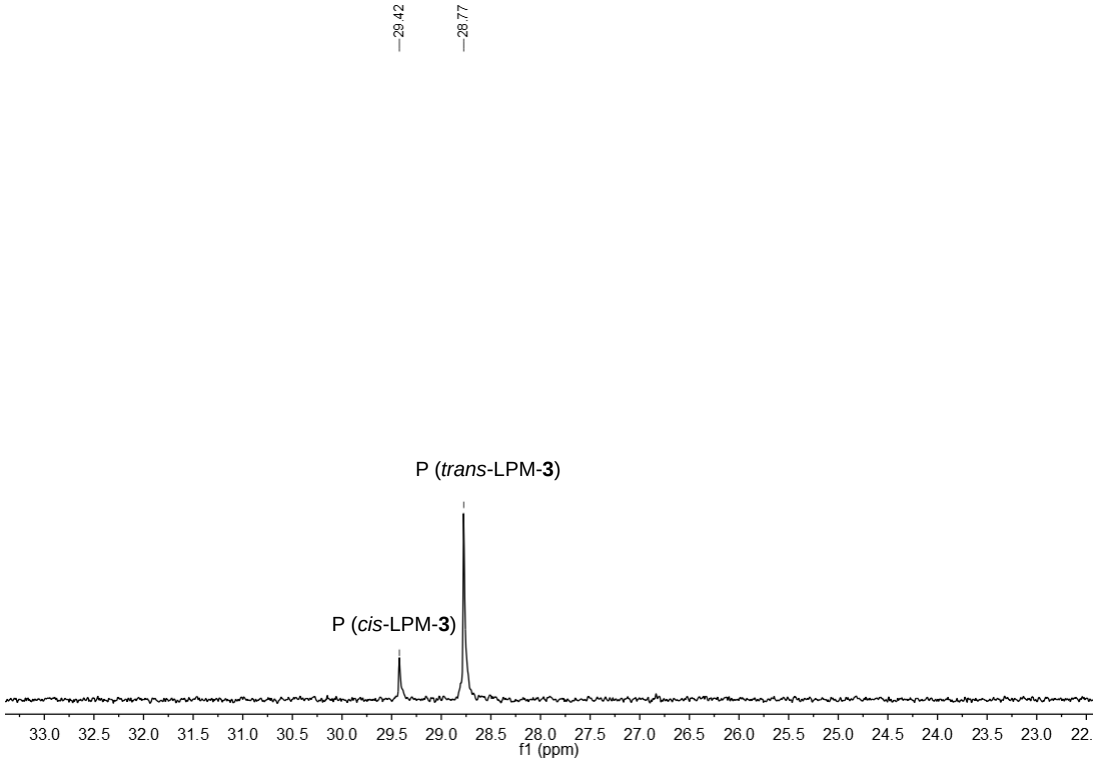

Fig. S29 ^{31}P NMR spectrum of LPM-**3** in C_6D_6 at 298 K

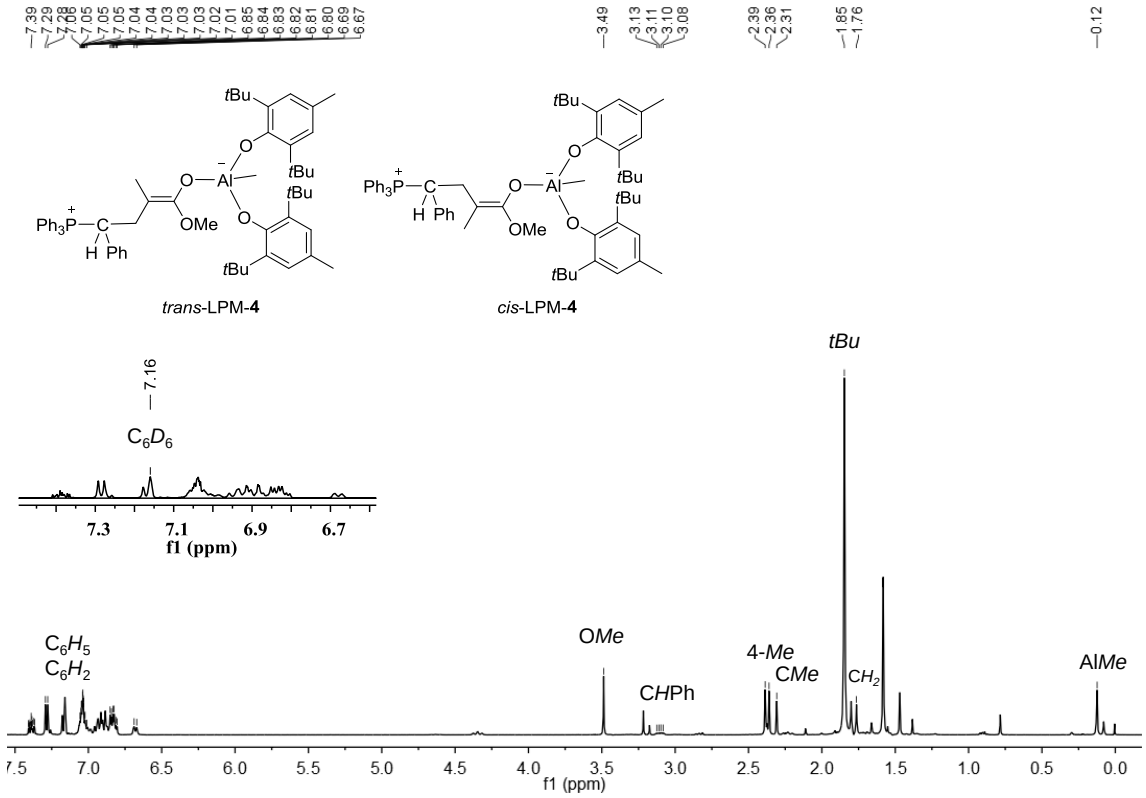

Fig. S30 ^{1}H NMR spectrum of LPM-**4** in C_6D_6 at 298 K (Note: the data were labeled for *trans*-LPM-**4**)

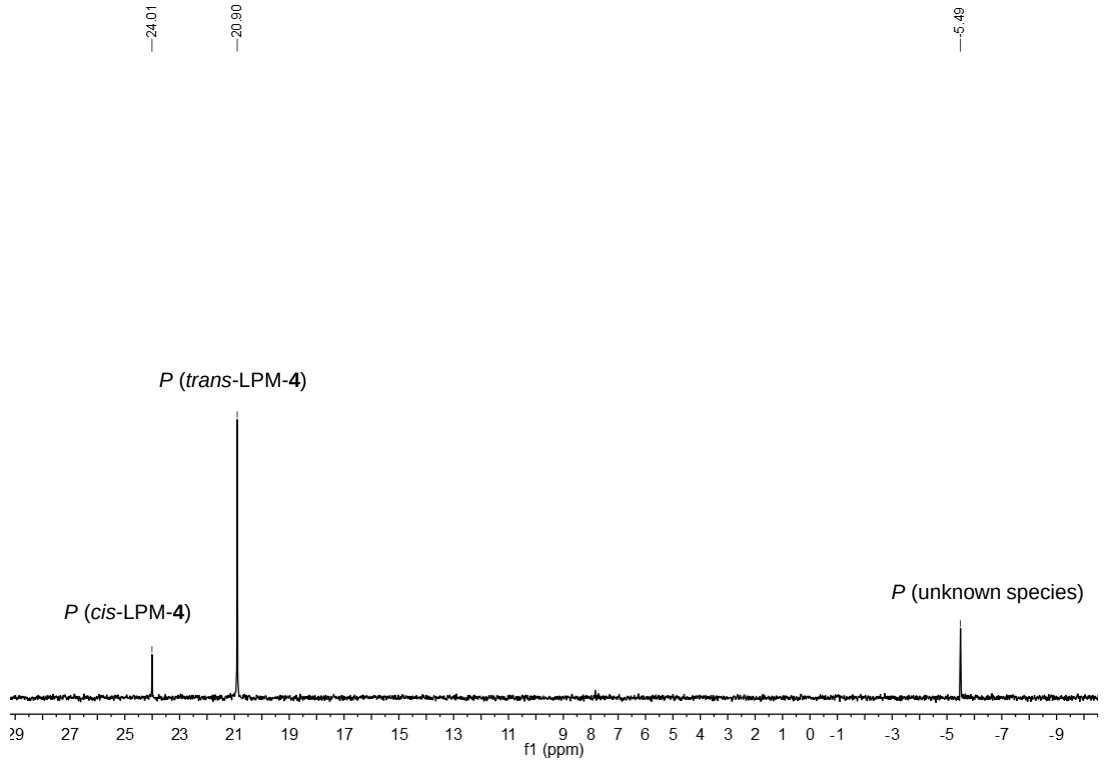

Fig. S31 ^{31}P NMR spectrum of LPM-**4** in C_6D_6 at 298 K

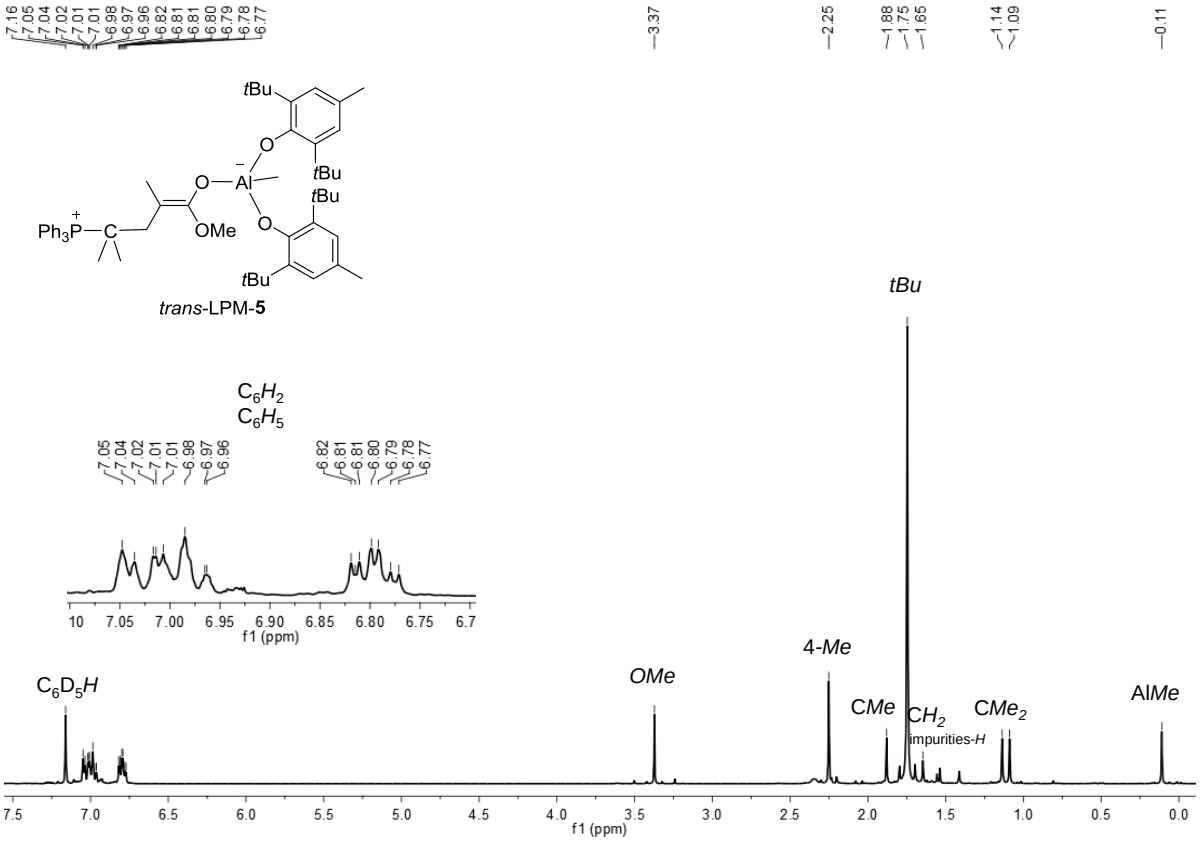

Fig. S32 ^{1}H NMR spectrum of LPM-**5** in C_6D_6 at 298 K

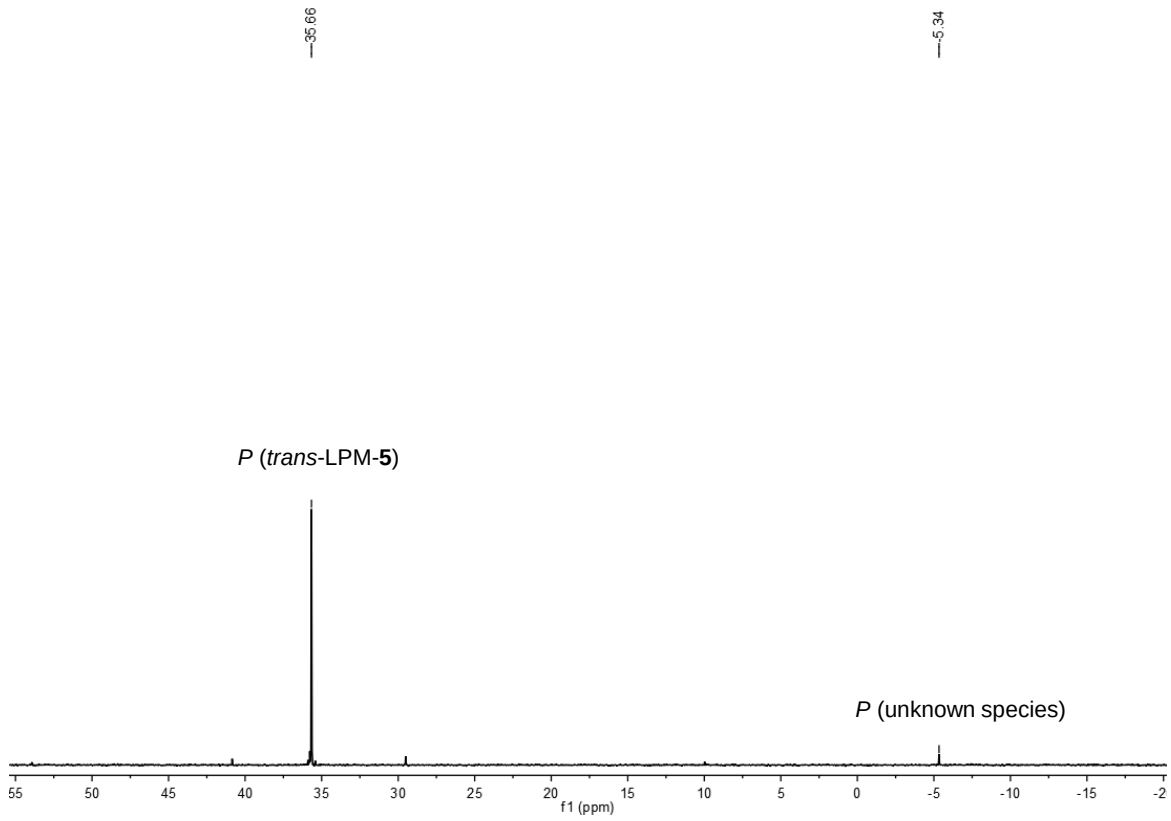

Fig. S33 ^{31}P NMR spectrum of LPM-**5** in C_6D_6 at 298 K

Ⅵ. References

1 G. M. Sheldrick, *Acta*. *Cryst. Sect. C*, 2015, **71**, 3–8.

2 G. M. Sheldrick, *Acta*. *Cryst. Sect. A,* 2008, **64**, 112–122.

3 M. A. Beckett, D. S. Brassington, S. J. Coles and M. B. Hursthouse, *Inorg. Chem. Commun.*, 2000, **3**, 530–533.

4 Z. M. Heiden and A. P. Lathem, *Organometallics*, 2015, **34**, 1818–1827.

5 Y. Zhao and D. G. Truhlar, *Theor. Chem. Acc.*, 2008, **120**, 215–241.

6 R. Krishnan, J. S. Binkley, R. Seeger and J. A. Pople, *J. Chem. Phys.*, 1980, **72**, 650–654.

7 M. J. Frisch, J. A. Pople and J. S. Binkley, *J. Chem. Phys*., 1984, **80**, 3265–3269.

8 A. E. Reed and F. Weinhold, *J. Chem. Phys.*, 1983, ***78***, 4066–4073.

9 A. E. Reed, R. B. Weinstock, F. Weinhold, *J. Chem. Phys.*, 1985, **83**, 735–746.

10 A. E. Reed, Weinhold, F. *J. Chem. Phys.,* 1985, **83**, 1736–1740.

11 A. E. Reed, L. A. Curtiss and F. Weinhold, *Chem. Rev*., 1988, **88**, 899–926.

12 J. E. Carpenter and F. Weinhold, *J. Mol. Struct*. *(Theochem)*, 1988, **46**, 41–62.

13 J. P. Foster and F. Weinhold, *J. Am. Chem. Soc.,* 1980, **102**, 7211–7218.

14 M. J. Frisch, G. W. Trucks, H. B. Schlegel, G. E. Scuseria, M. A. Robb, J. R. Cheeseman, G. Scalmani, V. Barone, B. Mennucci, G. A. Petersson, H. Nakatsuji, M. Caricato, X. Li, H. P. Hratchian, A. F. Izmaylov, J. Bloino, G. Zheng, J. L. Sonnenberg, M. Hada, M. Ehara, K. Toyota, R. Fukuda, J. Hasegawa, M. Ishida, T. Nakajima, Y. Honda, O. Kitao, H. Nakai, T. Vreven, J. J. A. Montgomery, J. E. Peralta, F. Ogliaro, M. Bearpark, J. J. Heyd, E. Brothers, K. N. Kudin, V. N.

Staroverov, R. Kobayashi, J. Normand, K. Raghavachari, A. Rendell, J. C. Burant, S. S. Iyengar, J. Tomasi, M. Cossi, N. Rega, J. M. Millam, M. Klene, J. E. Knox, J. B. Cross, V. Bakken, C. Adamo, J. Jaramillo, R. Gomperts, R. E. Stratmann, O. Yazyev, A. J. Austin, R. Cammi, C. Pomelli, J. W. Ochterski, R. L. Martin, K. Morokuma, V. G. Zakrzewski, G. A. Voth, P. Salvador, J. J. Dannenberg, S. Dapprich, A. D. Daniels, Ö. Farkas, J. B. Foresman, J. V. Ortiz, J. Cioslowski, D. J. Fox, *Gaussian 09*, Revision D.01; Gaussian, Inc.: Wallingford, CT, 2009.

END